EPR and Angle-Selected ENDOR Study of 5f-Ligand Interactions in the $[U(\eta^7\text{-}C_7H_7)_2]^-$ Anion, an f^1 Analogue of Uranocene

Didier Gourier,*,† Daniel Caurant,† Thérèse Arliguie,‡ and Michel Ephritikhine‡

Contribution from the Ecole Nationale Supérieure de Chimie de Paris, UMR-CNRS 7574, 11 rue Pierre et Marie Curie, 75231 Paris Cedex 05, France, and Service de Chimie Moléculaire, DSM, DRECAM, URA-CNRS 331, CEA CE Saclay, 91191 Gif sur Yvette, France

Received November 25, 1997

Abstract: A frozen solution of $[U(\eta^7\text{-}C_7H_7)_2]^-$ is studied by EPR and angle-selected ENDOR spectroscopy. EPR confirms the anticipated f^1 configuration of this compound. Analysis of the *g* tensor indicates that the ground state molecular orbital is principally made of $5f_\pi$ (51%) and $5f_\sigma$ (39%) uranium orbitals. This composition results from the combined effect of the spin−orbit interaction and the strong f_δ-ligand interactions. The small admixture of $5f_\phi$ (9%) uranium orbitals could result from a low-symmetry effect imposed by the solid-state packing forces at low temperature. Starting from the ground-state orbital, the f-level ordering consistent with the *g* tensor is found to be $(f_\pi,f_\sigma) < f_\phi < f_\pi < f_\phi$, $(f_\sigma,f_\pi) < f_\delta$ (antibonding). Proton ENDOR spectroscopy shows that there is a positive spin density $\rho_\pi \geq 4 \times 10^{-2}$ in $2p_\pi$ carbon orbitals, which manifests the covalent character of the ground-state orbital.

Introduction

Covalent contribution to the stability of organoactinide complexes has been widely studied since the discovery of uranocene $U(cot)_2$ ($cot = \eta^8\text{-}C_8H_8$) by Streitwieser and Müller-Westerhoff in 1968.[1] The interest of this compound is that its high symmetry D_{8h} due to the eclipsed ring conformation separates the contributions of the actinide 6d and 5f atomic orbitals (AO) to the molecular orbitals (MO), and thus simplifies the understanding of the metal−ligand interactions. This relatively simple molecular architecture motivated several theoretical calculations on uranocene and other actinocenes, including ligand field[2] and semiempirical nonrelativistic MO calculations.[3] However relativistic phenomena are important for actinide elements and numerous approaches have been used to investigate these effects, including ab initio complete active space self-consistent field,[4] quasirelativistic self-consistent field-X_α scattered wave,[5] discrete variational X_α,[6] linear combination atomic orbital Hartree−Fock−Slater,[7] relativistic extended Hückel,[8] and intermediate neglect of differential overlap[9] calculations.

This variety of theoretical approaches converges toward a general agreement concerning the extent of f-orbital participation to the metal−ligand bonding in actinocenes $M^{IV}(cot)_2$ (M = Th−Pu). In particular it is well-recognized that the actinide f_δ orbitals ($f_{z(x^2-y^2)}$,f_{xyz}) interact with the filled e_2'' MOs of C_8H_8 rings, while the other orbitals f_σ (f_{z^3}), f_π (f_{xz^2},f_{yz^2}) and f_ϕ ($f_{x(x^2-3y^2)}$,$f_{y(3x^2-y^2)}$)are localized and considered as nonbonding. In this context the f_δ orbitals are antibonding. The participation of $5f_\delta$ and $6d_\delta$ (d_{xy},$d_{x^2-y^2}$) to the bonding was nicely confirmed by Green et al. by photoelectron spectroscopy.[10]

Despite a good agreement between theoretical and photoelectron studies concerning the metal−ligand bonding, there is no clear experimental determination of the f-level ordering and the amount of interaction of f_σ, f_π, and f_ϕ AOs with ligand orbitals. This is because spin−orbit interaction and electron−electron repulsion considerably complicate the upper part of the energy level scheme of uranocene (f^2 configuration). Electron paramagnetic resonance (EPR) spectroscopy is very sensitive to spin−orbit effects, and its relatively high resolution compared to optical spectroscopies permits a precise determination of the orbital structure and the covalent character of the electronic ground states of paramagnetic compounds.[11] Compounds of the $M(cot)_2$ family with f^1 (protactinocene) and f^3 (neptunocene) configuration exhibit the Kramers degeneracy and should thus be EPR active. However it seems that these compounds have not been studied by this spectroscopy. Magnetic properties of actinocenes, in particular uranocene,[12] have been investigated by magnetic susceptibility measurements. However the inter-

† Ecole Nationale Supérieure de Chimie de Paris.

‡ Service de Chimie Moléculaire.

(1) Streitwieser, A.; Müller-Weisterhoff, U. *J. Am. Chem. Soc.* **1968**, *90*, 7634.

(2) (a) Hayes, R. G.; Edelstein, N. *J. Am. Chem. Soc.* **1972**, *94*, 8688. (b) Warren, K. D. *Inorg. Chem.* **1975**, *14*, 3095.

(3) Fischer, R. D. *Theor. Chim. Acta.* **1963**, *1*, 418.

(4) (a) Ortiz, J. V.; Hay, J.; Martin, R. L. *J. Am. Chem. Soc.* **1992**, *114*, 275. (b) Chang. A.; Pitzer, R. *J. Am. Chem. Soc.* **1989**, *111*, 2500.

(5) (a) Thornton, G.; Edelstein, N.; Rösch, N.; Egdell, R.; Woodward, D. *J. Chem. Phys.* **1979**, *70*, 5218. (b) Rösch, N.; Streitwieser, A., Jr. *J. Am. Chem. Soc.* **1983**, *105*, 7237.

(6) Kaltsoyannis, N.; Bursten, B. E. *J. Organomet. Chem.* **1997**, *528*, 19.

(7) Boerrigter, P. M.; Baerends, E. J.; Snijders, G. *J. Chem. Phys.* **1988**, *122*, 357.

(8) Pyykkö, P.; Lohr, L. L., Jr. *Inorg. Chem.* **1981**, *20*, 1950.

(9) Cory, M. G.; Köstlmeier, S.; Kotzian, M.; Rösch, M.; Zerner, M. C. *J. Chem. Phys.* **1994**, *100*, 1353.

(10) (a) Clark, J. P.; Green, J. *J. Organomet. Chem.* **1976**, *112*, C14. (b) Fragala, I. L.; Condorelli, G.; Zanella, P.; Tondello, E. *J. Organomet. Chem.* **1976**, *122*, 357. (c) Clark, J. P.; Green, J. C. *J. Chem. Soc., Dalton Trans.* **1977**, 505. (d) Brennan, J. G.; Green, J. C.; Redfern, C. M. *J. Am. Chem. Soc.* **1989**, *111*, 2373.

(11) Pilbrow, J. R. *Transition Ion Electron Paramagnetic Resonance*; Clarendon Press: Oxford, 1990.

(12) (a) Karraker, D. G.; Stone, J. A.; Jones, E. R.; Edelstein, N. *J. Am. Chem. Soc.* **1970**, *92*, 4841. (b) Karraker, D. G. *Inorg. Chem.* **1973**, *12*, 1105. (c) Edelstein, N.; La Mar, G. N.; Mares, F.; Streitwieser, A. *Chem. Phys. Lett.* **1971**, *8*, 399. (d) Amberger, H.; Fischer, R. D.; Kanellakopoulos, B. *Theor. Chim. Acta* **1975**, *37*, 105. (e) Dallinger, R. F.; Stein, P.; Spiro, T. G. *J. Am. Chem. Soc.* **1978**, *100*, 7865. (f) Jahn, W.; Yünlü, K.; Oroschin, W.; Amberger, H.; Fischer, R. *Inorg. Chim. Acta* **1984**, *95*, 85.

S0002-7863(97)04017-1 CCC: $15.00
Published on Web 06/05/1998

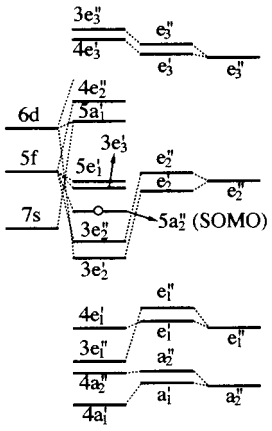

Figure 1. Partial energy level diagram of **1** (not to scale) after ref 14. The spin−orbit interaction is not considered.

pretation was rather ambiguous because of the multiplicity of states resulting from the combined effects of spin−orbit and electron−electron interactions.

The family of actinide sandwich compounds has been recently enriched since the discovery of the bis(cycloheptatrienyl)-uranium anion $[U(\eta^7\text{-}C_7H_7)_2]^-$ (**1**), synthesized in 1995 by Arliguie et al.[13] The interest of this complex is that it is the first *cycloheptatrienyl* sandwich compound and its ionic configuration should be $5f^1$ owing to the formal charge −3 of the C_7H_7 rings, which satisfies the $4n + 2$ rule for aromaticity, and thus implies a formal oxidation state V for uranium. A recent calculation by Li and Bursten showed that the ground-state configuration of **1** is a single electron in a localized uranium f orbital.[14] In this context **1** can be considered as the f^1 analogue of uranocene since MOs of the C_7H_7 rings have the same symmetries (in terms of group theory) as C_8H_8 rings.

A qualitative energy level diagram of **1**, taken from ref 14, is shown in Figure 1. The π-MOs of planar C_7H_7 rings span the irreducible representations $a_2'' < e_1'' < e_2'' < e_3''$ of the D_{7h} point group. Combination of the π-MOs of the two rings (in eclipsed configuration) gives MOs that are symmetric (a_1', e_1', e_2', e_3') and antisymmetric (a_2'', e_1'', e_2'', e_3'') with respect to the mirror plane perpendicular to the molecular axis.[14] The $6d_\delta$ and $5f_\delta$ AOs interact strongly with e_2' and e_2'' ligand MOs respectively, giving the filled bonding $3e_2'$ and $3e_2''$ MOs, so that **1** must be considered as a U^{III} rather than U^V compound.[14] Above these orbitals a series of 5f-based MOs with ordering $5a_2''$ (f_σ, 96%) < $3e_3'$ (f_ϕ, 97%) < $5e_1'$ (f_π, 92%) was found in a narrow energy range, followed by a 6d-based antibonding $5a_1'$ (d_{z^2}) MO and the strongly antibonding f-based $4e_2''$ (f_δ, 46%) MO. The ground-state configuration of **1** is thus $(3e_2')^4$ $(3e_2'')^4(f_\sigma)^1$, with one unpaired electron in a localized f orbital.[14] This compound should be characterized by an effective electron spin $S = {}^1/_2$ and should thus be EPR active.

However, as mentioned by Li and Bursten,[14] the sequence of the closely spaced f-based MOs can be modified by spin−orbit interactions, so that the description in terms of an unpaired electron in an f_σ orbital is only approximative. For this reason EPR is certainly the best tool for the study of the electron ground state of **1** because of its sensitivity to spin−orbit coupling effect.[11]

Even if the 5f-ring interaction is expected to be very small for σ, π, and ϕ orbitals,[4−9,14] a small amount of metal−ligand interaction should result in a resolved proton hyperfine (hf) structure in the EPR spectrum at high temperature since the ring rotation produces a motional narrowing of the hf lines.[15] However EPR of uranium compounds can only be observed in frozen solution and at very low temperatures because of the short spin−lattice relaxation time of actinides, so that ring proton hf interactions are not resolved in EPR, and in principle can only be revealed by ENDOR spectroscopy. This technique consists of an indirect detection of the NMR transitions of nuclei interacting with an electron spin. ENDOR spectra are obtained by partially saturating the EPR spectrum at a fixed magnetic field (the observing field) and sweeping a radio frequency radiation through nuclear resonance transitions.[16] It has been recognized that the ENDOR response of paramagnetic molecules diluted in frozen solution samples arises only from the subset of molecules responsible for the EPR intensity at the observing field.[17,18] When the anisotropy of the EPR spectrum is determined by the anisotropy of the g tensor, each observing field value $B_0 = h\nu/\beta g(\theta)$ corresponds to the selection of a subset of molecules with their symmetry axis making an angle θ with the magnetic field. Such angle-selected ENDOR spectroscopy gives the hf parameters with high accuracy.[17,18]

In this paper we present a combined EPR−ENDOR study of **1** in frozen solution, with the purpose of determining the 5f and ligand orbital composition of the SOMO (singly occupied molecular orbital), and to obtain information about the f-level ordering. This work proceeds in three steps: (a) the 5f composition of the SOMO is first determined from the EPR spectrum. The SOMO is greatly influenced by spin−orbit coupling effects since it is mainly f-based, so that we analyzed the EPR in the weak field approximation, which is the most suitable for situations where spin−orbit effects dominate interactions with ligands. In this case the total angular momentum J is a good quantum number and we first describe the ground state in terms of $|J,M_J\rangle$ states, where M_J is the z component of J. The transformation into the usual f-orbital representation is made by a unitary tranformation. (b) In a second step the f-level ordering is deduced from the analysis of the SOMO, by identifying the combined effects of the spin−orbit and the f-ligand interactions. (c) In the last step the covalent character of the SOMO is studied by angle-selected ENDOR spectroscopy, which gives the spin density in 1s hydrogen and 2p carbon orbitals.

Experimental Section

1 was synthesized as described in ref 13. A quartz tube was filled with ∼1−5 mg of **1** dissolved in 0.4 mL of α-methyl-THF, and sealed under vacuum. Frozen solution X-band EPR spectra were recorded below 15 K with a Bruker ESP 300e spectrometer equipped with an Oxford intrument ESR 9 continuous flow helium cryostat. ENDOR spectra were recorded at 4 K with the Bruker ENDOR cavity working in the TM_{110} mode. The radio frequency (rf) field was amplified by a 100W ENI broad-band power amplifier. A 12.5 kHz frequency modulation of the rf carrier (modulation depth 70 kHz) was used for

(13) Arliguie, T.; Lance, M.; Nierlich, M.; Vigner, J.; Ephritikhine, M. *J. Chem. Soc., Chem. Commun.* **1995**, 183.

(14) Li, J.; Bursten, B. E. *J. Am. Chem. Soc.* **1997**, *119*, 9021.

(15) In transition metal sandwich compounds, the rapid reorientation of planar rings around the molecular axis induces a partial averaging of the proton hf interaction, and the principal axes of the g tensor and the averaged hf tensor become collinear. For this reason the proton hf interaction of sandwich compounds is generally well-resolved in liquid solution and in frozen solution at temperatures larger than above 100 K. See for example Gourier, D.; Samuel, E.; Bachmann, B.; Hahn, F.; Heck, J. *Inorg. Chem.* **1992**, *31*, 86.

(16) Feher, G. *Phys. Rev.* **1956**, *103*, 834.

(17) (a) Rist, G. H.; Hyde, J. S. *J. Chem. Phys.* **1970**, *52*, 4633. (b) Hoffman, B. M.; Martinsen, J.; Venters, R. A. *J. Magn. Reson.* **1984**, *59*, 110.

(18) Hurst, G. C.; Henderson, T. A.; Kreilick, R. W. *J. Am. Chem. Soc.* **1985**, *107*, 7294.

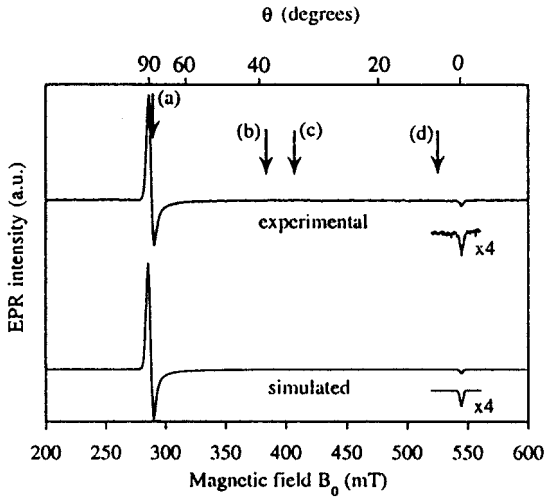

Figure 2. Frozen solution EPR spectrum at 15 K of **1**, compared with a simulated spectrum. The arrows indicate the four selected field setting values corresponding to ENDOR spectra of Figure 5.

the detection. With this modulation scheme, the ENDOR signal takes the form of the first derivative of the ENDOR enhancement. A moderate microwave power (≈6 mW) was sufficient to optimize the ENDOR intensity.

Electron Paramagnetic Resonance Spectroscopy

(1) Determination of the 5f Composition of the SOMO. Figure 2 shows a frozen solution EPR spectrum of **1** at 15 K. It exhibits a typical axial powder line shape of a $S = {}^1/_2$ molecule, with an intense turning point corresponding to the molecular orientations $\mathbf{B}_0 \perp z$ and a small one at high field for $\mathbf{B}_0 \parallel z$, where z is the molecular axis. This interpretation was verified by simulation which accurately reproduced the experimental line shape.[19] The principal values of the g tensor are $g_{\parallel} = 1.244 \pm 0.005$ and $g_{\perp} = 2.365 \pm 0.005$. It is important to note that the simulation is independent of the sign of the g factors, so that the latter will be considered positive throughout the paper. In principle, it could be possible to determine the sign of the product $g_x g_y g_z$ by using a circularly polarized microwave field.[20] The shape of the EPR spectrum confirms the anticipated $5f^1$ configuration of **1**.[13,14] However the g values do not agree with the expected ground-state configuration $(f_\sigma)^1$ calculated by neglecting the spin−orbit interaction,[14] because an electron in a $M_l = 0$ orbital (which is the case with f_σ) does not experience spin−orbit interaction for the field orientation $\mathbf{B}_0 \parallel z$, so that $g_{\parallel}$ should be equal to the free spin value $g_e = 2.002$. This is not the case with **1**. This discrepancy originates from the fact that spin−orbit effects should modify significantly the energy level scheme in the energy range of localized f-based orbitals.[14] We must thus analyze the experimental g-factors by taking into account the spin−orbit interaction simultaneously with metal−ligand interactions.

The metal−ligand interaction in transition metal compounds is of the same order of magnitude as the spin−orbit interaction, and it is often possible to extract the metal AO composition of the SOMO from the g tensor, and the amount of metal−ligand interaction from both the g tensor and the hf interactions.[11,20] However most of the 5f metal AOs are assumed to be essentially nonbonding in actinide sandwich compounds,[2−9,14] so that the strong spin−orbit interaction of the metal should largely dominate the weak metal−ligand interactions. Consequently the $5f^1$ configuration of **1** should be more conveniently treated in the weak field approximation, with states $|(5f^1),L{=}3,S{=}{}^1/_2,J,M_J\rangle$ (hereafter referred to as $[|J,M_J\rangle]$ representation) characterized by the total angular momentum $J = L + S, L + S - 1, ..., |L - S| = {}^7/_2, {}^5/_2$ and its projection $M_J = J, J - 1, ..., -J$ along the z axis. Once the $|J,M_J\rangle$ composition of the SOMO is determined from the analysis of g factors, it can be transformed into the f orbital representation, characterized by states $|(5f^1),L{=}3,S{=}{}^1/_2,M_L,M_S\rangle$ (hereafter referred to as $[|M_L,M_S\rangle]$ representation) where $M_L = \pm 3, \pm 2, \pm 1, 0$ and $M_S = \pm {}^1/_2$ are the z projections of the orbital and spin momentum. The f_σ, f_π, f_δ, and f_ϕ orbitals correspond respectively to $|M_L| = 0, 1, 2, 3$. Passing from $[|J,M_J\rangle]$ to $[|M_L,M_S\rangle]$ representation is achieved by the unitary transformation $|J,M_J\rangle = \sum_{M_L,M_S}\langle M_L,M_S|J,M_J\rangle|M_L,M_S\rangle$ where parameters $\langle M_L,M_S|J,M_J\rangle$ are the Clebsch-Gordan coefficients.[21] Table 1 represents the composition (in %) of the atomic $|J,M_J\rangle$ states in terms of f_σ, f_π, f_δ, and f_ϕ orbitals.

Table 1. Composition (in %) in f_σ, f_π, f_δ, and f_ϕ Orbitals of the $|J,M_j\rangle$ States of a f^1 Configuration

$[\|J,M_j\rangle]$ representation		$[\|M_l,M_s\rangle]$ representation			
J	M_j	f_σ (%)	f_π (%)	f_δ (%)	f_ϕ (%)
	$^7/_2$				100
$^7/_2$	$^5/_2$			85.8	14.2
	$^3/_2$		71.4	28.6	
	$^1/_2$	57.1	42.9		
	$^5/_2$			14.2	85.8
$^5/_2$	$^3/_2$		28.6	71.4	
	$^1/_2$	42.9	57.1		

Let us first consider the effect of the spin−orbit interaction on the f^1 configuration of **1**. This removes the degeneracy of the $^{2S+1}L = {}^2F$ ground state and gives two states $^2F_{5/2}$ and $^2F_{7/2}$ characterized by $J = {}^5/_2$ and $^7/_2$, respectively. The energy splitting between the ground state $J = {}^5/_2$ and the excited state $J = {}^7/_2$ of the free U^V ion is equal to $7\lambda/2 = 7608\ cm^{-1}$.[22] The three principal effects of the metal−ligand interactions are (i) the removal of the $2J + 1$ degeneracy of $^2F_{5/2}$ and $^2F_{7/2}$ states to doubly degenerate Kramers states, (ii) the second-order mixing of states with different J and the same M_J values, and (iii) a ligand admixture in the SOMO. However iii should be relatively small and i should largely dominate effect ii because of the important energy splitting between $^2F_{5/2}$ and $^2F_{7/2}$ states, so that the main consequence of the metal−ligand interaction is the removal of the 6-fold degeneracy of the $^2F_{5/2}$ ground state into three Kramers doublets. As a consequence $J = {}^5/_2$ may be considered as a good quantum number in a first-order treatment. At this level of approximation the ligand effects can be described by the ligand field operator:[20]

$$H_c = \sum_{k=0}^{2J} \sum_{q=-k}^{+k} B_k^q O_k^q \qquad (1)$$

where B_k^q and O_k^q are the ligand field parameters and the spin operators, respectively. If the ligand field splitting is much larger than kT and the Zeeman energy, only the lowest Kramers doublet is populated and the system can be treated as an effective $\tilde{S} = {}^1/_2$ spin doublet. The two normalized wave functions $|\pm\rangle = |\tilde{S},\tilde{M}_S = \pm {}^1/_2\rangle$ of a Kramers doublet are written as linear combinations of $|J,M_J\rangle$ states characterized by different M_J

(19) Spectra were simulated with the WIN-EPR SimFonia simulation program from Bruker. The simulations used Gaussian line shape functions with line width $\Delta B_{\parallel} = 2.5$ mT and $\Delta B_{\perp} = 4.0$ mT.

(20) Abragam, A.; Bleaney, B. *Electron Paramagnetic Resonance of Transition Metal Ions*; Clarendon Press: Oxford, 1971.

(21) Brandsen, B. H.; Joachain, C. J. *Introduction to Quantum Mechanics*; Wiley: New York, 1995.

(22) Kaufman, V.; Radziemski, L. J. *J. Opt. Soc. Am.* **1976**, *66*, 599.

values:[20]

$$|+\rangle = \sum_{M_J} a_{M_J}|J,M_J\rangle$$

$$|-\rangle = \sum_{M_J}(-1)^{J-M_J}\, a^*_{M_J}|J,-M_J\rangle \qquad (2)$$

with

$$1 = \sum_{M_J}|a_{M_J}|^2$$

where the nonzero values of a_{M_J} in the summations are only determined by the symmetry of the compound. The residual degeneracy $2\tilde{M}_S + 1 = 2$ of the Kramers doublets is lifted by the external magnetic field $\mathbf{B}_0$, which gives the following spin Hamiltonian of the effective spin $\tilde{S} = {}^1/_2$ coupled to proton spins $I = {}^1/_2$ by the hf interaction:

$$H_Z = \beta\tilde{\mathbf{S}}\cdot\bar{\bar{\mathbf{g}}}\cdot\mathbf{B}_0 + \sum_{k=1}^{14}\mathbf{S}\cdot\bar{\bar{\mathbf{A}}}_\mathbf{k}\cdot\mathbf{I}_\mathbf{k} \qquad (3)$$

where $\bar{\bar{\mathbf{g}}}$ and $\bar{\bar{\mathbf{A}}}_\mathbf{k}$ are the g tensor and the hf tensor for the kth proton. The principal values g_x, g_y, and g_z of the g tensor are functions of the coefficients a_{M_J} in expressions 2.

Complex **1** with the eclipsed conformation has the D_{7h} symmetry. However X-ray diffraction and theoretical calculations showed that it exhibits the staggered conformation.[13,14] The latter should have the D_{7d} (or D_7) symmetry in the gas phase, but this symmetry is actually reduced to C_{2h} in the solid state,[13] presumably because of the crystal packing forces. Despite the fact that such forces may exist in frozen solution, we shall first analyze the g tensor by considering the axial D_{7h}, D_{7d}, or D_7 symmetries. It has been demonstrated that any l^x configuration with C_n, C_{nh}, C_{nv}, D_n, D_{nh}, and D_{nd} symmetry can be treated in terms of a field of effectively axial $C_{\infty v}$ symmetry as long as $n \geq 2l + 1$.[2,23] Thus both the eclipsed and the gas-phase staggered conformations of **1** may be treated in $C_{\infty v}$ symmetry. In this case all the B^q_k coefficients with $q \neq 0$ vanish in eq 1 and the remaining spin operators O^0_2 and O^0_4 are only functions of J^2_z and J^4_z operators, so that H_c is diagonal in the $[|J,M_J\rangle]$ representation. The effect of H_c is to remove, without mixing, the degeneracy of the three Kramers doublets. The three pairs of wave functions of the effective $\tilde{S} = {}^1/_2$ spin doublets are given by expression 2 with only one nonzero value of a_{M_J}, which thus become $|\pm\rangle = |J,\pm M_J\rangle$. The three Kramers doublets are characterized by axial g factors, with the two components given by

$$\begin{aligned}
&|{}^5/_2,\pm{}^1/_2\rangle \qquad g_\parallel = g_J = 0.86 \\
&\qquad\qquad\qquad\quad g_\perp = 3g_J = 2.57 \\
&|{}^5/_2,\pm{}^3/_2\rangle \qquad g_\parallel = 3g_J = 2.57 \\
&\qquad\qquad\qquad\quad g_\perp = 0 \\
&|{}^5/_2,\pm{}^5/_2\rangle \qquad g_\parallel = 5g_J = 4.29 \\
&\qquad\qquad\qquad\quad g_\perp = 0
\end{aligned} \qquad (4)$$

where $g_J = {}^6/_7$ is the Landé factor for a $^2F_{5/2}$ state.

The experimental sequence of g parameters $g_\perp > 2 > g_\parallel > 0$ measured for **1** is close to the theoretical values $g_\perp = 3g_\parallel = 2.57$ expected for the $|{}^5/_2,\pm{}^1/_2\rangle$ state, and very different from the sequence $g_\parallel > 2 \gg g_\perp = 0$ expected for the two other doublets of states, so that we may deduce that the ground state Kramers doublet is essentially made of the $|M_j| = {}^1/_2$ states. However the difference between experimental and theoretical g values is sufficiently important to imply that the predominantly $|{}^5/_2,\pm{}^1/_2\rangle$ ground state is mixed with other $|J,\pm M_J\rangle$ states. In pseudoaxial symmetry, this effect may result from a second-order admixture of the $^2F_{7/2}$ state, which is accounted for by adding a term $B^0_6\,O^0_6$ to the allowed $B^0_2\,O^0_2$ and $B^0_4\,O^0_4$ terms in eq 1, which admixes the $|{}^7/_2,\pm{}^1/_2\rangle$ states in the $|{}^5/_2,\pm{}^1/_2\rangle$ ground state. The theoretical expressions for the components of the g factor become in that case:[20]

$$g_\parallel = 2\sin^2\theta$$

$$g_\perp = 2|\sqrt{3}\sin 2\theta - \sin^2\theta| \qquad (5)$$

However it was not possible to find a value for θ which satisfies eq 5. For example $\theta = 52.06°$ gives the accurate value of $g_\parallel$, but gives also $g_\perp = 2.113$, a value significantly different from the experimental value $g_\perp = 2.365$. Consequently the purely $|M_j| = {}^1/_2$ ground state is not able to fit the experimental values of the axial g tensor of **1**, even by considering second-order effects. We must thus consider other admixtures to the predominantly $|{}^5/_2,\pm{}^1/_2\rangle$ ground state. Such effects are possible if solid-state packing forces are also effective in frozen solution. For example if the symmetry is lowered to C_{2h}, as it was effectively found in the solid state by X-ray diffraction,[13] the first-order crystal field operator is given by eq 1 with $J = {}^5/_2$ and the symmetry allowed values of k and q[24] where O^2_2 and

$$H_c = B^0_2\,O^0_2 + B^2_2\,O^2_2 + B^0_4\,O^0_4 + B^2_4\,O^2_4 + B^4_4\,O^4_4 \qquad (6)$$

O^2_4 operators contain $S^2_\pm$ spin operators which mix M_J states differing by 2, so that the ground-state wave function is now written as

$$|\pm\rangle = \pm a|{}^5/_2,\pm{}^1/_2\rangle \pm b|{}^5/_2,\pm{}^5/_2\rangle \pm c|{}^5/_2,\mp{}^3/_2\rangle \qquad (7)$$

with $a^2 + b^2 + c^2 = 1$. The operator O^4_4 mixes M_J states differing by 4, so that the term $B^4_4\,O^4_4$ produces only a second-order admixture in the $|{}^5/_2,\pm{}^1/_2\rangle$ state and is thus neglected. The wave function 7 is characterized by a rhombic g tensor expressed as[25]

$$\begin{aligned}
g_x &= \pm{}^6/_7(2\sqrt{5}bc + 4\sqrt{2}ac + 3a^2) \\
g_y &= \pm{}^6/_7(2\sqrt{5}bc - 4\sqrt{2}ac + 3a^2) \\
g_z &= \pm{}^6/_7(5b^2 + a^2 - 3c^2)
\end{aligned} \qquad (8)$$

The experimental g values satisfy expressions 8 for the following ground-state wave function in the $[|J,M_J\rangle]$ representation:

$$|\pm\rangle = \pm 0.948|{}^5/_2,\pm{}^1/_2\rangle \pm 0.323|{}^5/_2,\pm{}^5/_2\rangle \qquad (9)$$

which gives the two g values $g_z = g_\parallel = 1.215$ and $g_x = g_y = g_\perp = 2.311$ close to the experimental results (Table 2). The parameters $g_\parallel$ and $g_\perp$ deduced from eq 9 have the same sign, which is thus taken positive. Because the admixture of M_j states

(23) Scott, D. R.; Matsen, F. A. *J. Phys. Chem.* **1968**, *72*, 16.

(24) Misra, S. K.; Poole, C. P.; Farach, H. A. *Appl. Magn. Reson.* **1996**, *11*, 29.

(25) McLaughlan, F. D.; Forrester, P. A. *Phys. Rev.* **1966**, *151*, 311.

Table 2. Spin Hamiltonian Parameters of **1**[a]

$g_{\|}$	$g_{\perp}$	A_1	A_2	A_3	A_{iso}	A_1^{aniso}	A_2^{aniso}	A_3^{aniso}
1.244 ± 0.005	2.365 ± 0.005	−5.8(5)	−5.5(9)	+3.3(3)	−2.7(0)	−3.1(5)	−2.8(9)	+6.0(3)

[a] Hyperfine parameters are given in MHz.

into the ground state should be inversely proportional to the splitting ΔE between these states, the relative importance of the $|^5/_2,\pm^5/_2\rangle$ admixture in the $|^5/_2,\pm^1/_2\rangle$ ground state compared to the lack of admixture of $|^5/_2,\pm^3/_2\rangle$ indicates that in axial symmetry (D_{7h}, D_{7d}, or D_7) the $|^5/_2,\pm^5/_2\rangle$ Kramers doublet is probably very close to the ground state $|^5/_2,\pm^1/_2\rangle$, while the $|^5/_2,\pm^3/_2\rangle$ state is removed at higher energy. It will be shown below that this feature is a direct consequence of the antibonding character of the f_δ orbital.

The passage of the wave function (eq 9) from the $[|J,M_J\rangle]$ representation to the $[|M_l,M_s\rangle]$ representation is achieved by using Clebsch−Gordan coefficients (see also Table 1):

$$|\pm\rangle = \mp 0.621|0,\pm^1/_2\rangle \pm 0.717|\pm 1,\mp^1/_2\rangle \mp 0.122|\pm 2,\pm^1/_2\rangle \pm 0.298|\pm 3,\mp^1/_2\rangle \quad (10)$$

Thus the electron ground state of **1** is mainly composed of $5f_\sigma$ (38.5%) and $5f_\pi$ (51.4%) metal orbitals, with a small admixture of $5f_\phi$ (8.9%) and $5f_\delta$ (1.5%) orbitals.

(2) Determination of the f-Level Ordering. The rather complicated f-orbital composition (expression 10) of the ground-state wave functions results from the combination of three effects: (i) the spin−orbit interaction, (ii) the metal ligand interaction, and (iii) the actual symmetry of the complex which produces the admixture of $|M_j| = {}^5/_2$ into the $|M_j| = {}^1/_2$ ground state. In pseudoaxial symmetry, the ground state would be of purely $|M_j| = {}^1/_2$ character, which is written in $[|M_l,M_s\rangle]$ representation as

$$|^5/_2,\pm^1/_2\rangle = \pm 2/\sqrt{7}|\pm 1,\mp^1/_2\rangle \mp \sqrt{^3/_7}|0,\pm^1/_2\rangle \quad (11)$$

thus with a composition of $5f_\pi$ (57.1%) and $5f_\sigma$ (42.9%) AOs which is close to that found for the actual ground state of **1**. A 2-fold symmetry allows admixture of both $|M_j| = {}^5/_2$ and ${}^3/_2$ in the ${}^1/_2$ ground state although only ${}^5/_2$ was found experimentally. As mentioned above this feature points to an energy level ordering $|M_j| = {}^1/_2 < {}^5/_2 \ll {}^3/_2$ for the axial symmetry of **1** in the gas phase. However a ligand field calculation[2] predicted that the energy level ordering of the f^1 configuration of actinocenes with pseudoaxial symmetry should be $|M_j| = {}^5/_2 < {}^1/_2 < {}^3/_2$, for which we expect a sequence of g factors $g_{\|} > 2 \gg g_\perp > 0$ very different from the experimental one $g_\perp > 2 > g_{\|} > 0$. Moreover, without spin−orbit interaction, the ground-state wave function of **1** should be of purely $|M_l,M_s\rangle = |0,\pm^1/_2\rangle$ (f_σ) character,[14] for which we predict a parallel g factor $g_{\|} = 2.002$ very different from the experimental value $g_{\|} = 1.244$.

It will be shown that the f-orbital composition (eq 10) of **1** is the result of a combined effect of the spin−orbit interaction and the strong $f_\delta - e_2''$ interaction, which was predicted to dominate the upper part of the energy level diagram of actinocenes.[7] Up to now we analyzed the g tensor in the weak field approximation without a particular hypothesis on the f-ligand interactions. The spin−orbit operator

$$H_{SO} = \lambda \mathbf{L}\cdot\mathbf{S} = \frac{\lambda}{2}[J^2 - L^2 - S^2] \quad (12)$$

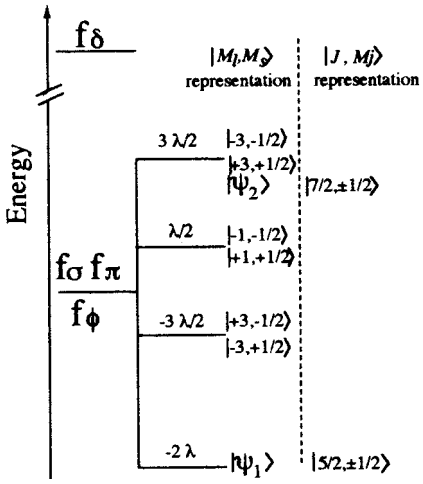

Figure 3. First-order effect of spin−orbit interaction on a degenerate set of f_σ, f_π, and f_ϕ orbitals. The resulting states are given in $[|M_l,M_s\rangle]$ representation, and also in $[|J,M_j\rangle]$ representation when J may characterize a particular state. The composition of states $|\psi_1\rangle$ and $|\psi_2\rangle$ is given in expressions 14.

was thought to occur on a complete f-AOs set, written in the $[|J,M_j\rangle]$ representation since J is a good quantum number in that case and is supposed to give a degenerate $^2F_{5/2}$ ground state in spherical symmetry. This degeneracy was lifted into Kramers doublets only by the metal−ligand interactions. This picture is not correct if one of the f-AOs, namely the $5f_\delta$, participate to the metal−ligand bonding with the $3e_2''$ (bonding) and the $4e_2''$ (antibonding) MOs (Figure 1). In this case J is no longer a good quantum number, and spin−orbit interaction should be studied in the $[|M_l,M_s\rangle]$ representation by using only the orbital and spin operators in H_{SO}:[7]

$$H_{SO} = \lambda L_z S_z + \frac{\lambda}{2}(L^+S^- + L^-S^+) \quad (13)$$

Figure 3 shows the effect of the spin−orbit interaction on the degenerate set of f_σ, f_π, and f_ϕ orbitals by a first-order perturbation calculation. Due to their strong covalent character, the f_δ orbitals are involved in bonding and antibonding orbitals and are not considered in the calculation because of their important splitting from the other f orbitals, so that they interact with the f_σ, f_π, and f_ϕ AOs only in a second-order correction. The different states resulting from the spin−orbit interaction, written in the $[|M_l,M_s\rangle]$ representation, are also written in the $[|J,M_j\rangle]$ representation when J remains a good quantum number for the description of a particular level. It can be seen that spin−orbit interaction mixes only the f_σ and the two f_π orbitals characterized by M_l and M_s of opposite sign. The $\sigma-\pi$ mixing gives two levels $|\psi_1\rangle$ and $|\psi_2\rangle$ at -2λ and $+3\lambda/2$ respectively:

$$|\psi_1\rangle = \mp\sqrt{^3/_7}|0,\pm^1/_2\rangle \pm 2/\sqrt{7}|\pm 1,\mp^1/_2\rangle$$
$$|\psi_2\rangle = \pm 2/\sqrt{7}|0,\pm^1/_2\rangle \pm \sqrt{^3/_7}|\pm 1,\mp^1/_2\rangle \quad (14)$$

which correspond to the pure $|J,M_J\rangle = |^5/_2,\pm^1/_2\rangle$ and $|^7/_2,\pm^1/_2\rangle$ states respectively (see Table 1). The ground state doublet $|\psi_1\rangle$ is followed by a closely spaced doublet made of f_ϕ orbitals with M_l and M_s of opposite signs, located at $\lambda/2$ above $|\psi_1\rangle$. This splitting can be smaller than $\lambda/2$ if $|\psi_1\rangle$ exhibits an antibonding character, as will be shown by ENDOR. The next doublet at $5\lambda/2$ above $|\psi_1\rangle$ is of purely f_π character with M_l and M_s being of the same sign. The highest energy levels are two degenerate doublets at $7\lambda/2$ above $|\psi_1\rangle$, the first one being $|\psi_2\rangle$ and the other ones being of purely f_ϕ character, with M_l and M_s of the same sign. At this stage the main characteristics of the electron ground state orbitals of **1** (expression 10) deduced from the analysis of the *g* tensor can be interpreted as follows:

(a) In "spherical" symmetry, the combined effects of the spin−orbit interaction and the strong covalent character of the $f_\delta - e_2''$ interaction result in a doubly degenerate ground state composed of f_π (≈57%) and f_σ (≈43%) orbitals. This composition is similar to that of the SOMO of **1**. There is a close excited doubly degenerate level composed of pure f_ϕ orbitals. The sequence of f levels should be $(f_\pi, f_\sigma) < f_\phi < f_\pi < f_\phi, (f_\pi, f_\sigma)$.

(b) The f-ligand interactions with the pseudoaxial symmetry of the gas-phase staggered conformation of **1** would shift without mixing the energy levels. However this effect is probably small since there is no level inversion and $|\psi_1\rangle$ remains the ground-state doublet.

(c) The actual low symmetry due to the combined effects of the staggered conformation and the solid-state packing forces induces a mixing of the ground state $|\psi_1\rangle$ orbitals with the closely spaced f_ϕ orbitals. The low symmetry also allows a f_δ admixture. However the f_ϕ admixture (≈9%) is much larger than that of f_δ (≈1%), because the amount of mixing being inversely proportional to the energy splitting between the orbitals, this favors a mixing with the closely spaced f_ϕ AOs rather than with the f_δ orbitals participating in the bonding and antibonding $3e_2''$ and $4e_2''$ MOs.

Electron Nuclear Double Resonance Spectroscopy

In this part we analyze the ligand contribution to the SOMO by ENDOR spectroscopy. Only the 14 hydrogen atoms possess a nuclear spin so that ENDOR should give information only about the uranium−hydrogen hyperfine interactions. However the 5f-C_7H_7 covalency should result in an unpaired spin density in $2p_\pi$ carbon orbitals, which in turn should produce a spin density on hydrogen 1s orbitals by spin polarization. Thus the proton hf interaction contains information on the f-carbon covalent interactions.

Three kinds of interactions are responsible for an unpaired spin density on ligand orbitals.[26] Figure 4 represents a schematic energy level diagram with two f-based uranium orbitals (f_1 and f_2), the lowest one (f_1) with a single electron, and two ligand-based MOs made of symmetry-adapted linear combination of carbon p_π orbitals ($l_{\pi1}$ and $l_{\pi2}$). This diagram represents also one of the CH-based σ orbitals of the C_7H_7 rings. The uranium−ligand interaction manifests itself either by a virtual electron transfer from the ligand $l_{\pi1}$ MO to one of the uranium f orbitals (mechanisms a and b) or by a transfer from the metal f_1 orbital to the empty ligand $l_{\pi2}$ MO by the back-bonding mechanism (c). If the ligand-to-metal transfer occurs in the singly occupied uranium orbital f_1, only a spin $m_s = -^1/_2$ can be transferred because of the Pauli principle, leaving a positive spin density $\rho_\pi > 0$ in p_π carbon orbitals (Figure 4a). If the electron transfer occurs in the empty uranium orbital f_2, both

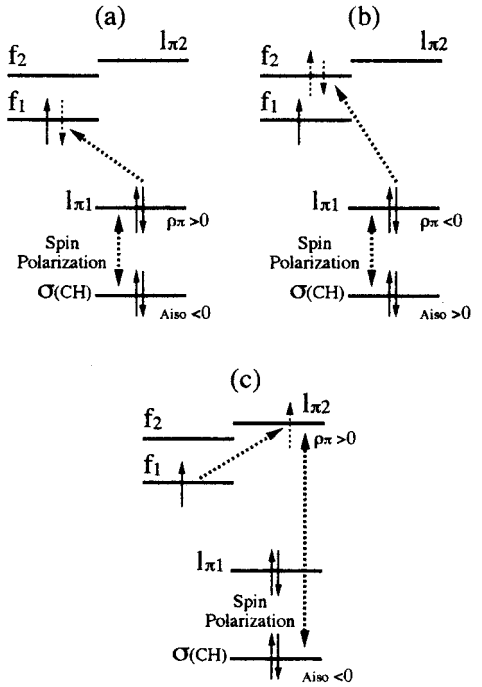

Figure 4. Simplified energy level diagram showing the three types of covalent transfer giving an unpaired spin density in $2p_\pi$ carbon orbital, which in turn induces an isotropic proton hf interaction A_{iso} by spin polarization of the inner CH-based MOs. (a) ligand to half-filled metal orbital transfer; (b) ligand to empty metal orbital transfer; and (c) metal to ligand transfer (back-bonding).

$m_s = \pm^1/_2$ electrons can be transferred. However because of the exchange energy, the transfer is more favorable for the $m_s = +1/2$ electron than for the other, so that this exchange-polarized transfer leaves a negative spin density $\rho_\pi < 0$ on carbon p_π orbitals (Figure 4b). It is evident that the back-donation mechanism (c) leads to $\rho_\pi > 0$. Thus the determination of the sign and magnitude of ρ_π should give information about the nature of the covalent interactions involving the SOMO and the unoccupied f-based orbitals.

A direct measurement of ρ_π is not possible because only the ^{13}C isotope possesses a nuclear spin $I = ^1/_2$, and its very low natural abundance (1.11%) precludes its detection by frozen solution ENDOR. However a spin density ρ_π on carbon p_π orbitals polarizes the inner CH-based σ orbitals.[27] A positive spin density $\rho_\pi = +1$ should result in an exces of negative spin density at the hydrogen nucleus, responsible for a negative proton hf interaction of about −80 MHz, the exact value depending on the arene molecule. Thus an accurate measurement by ENDOR of the magnitude and sign of the proton hf interaction should give an estimate of ρ_π.

(1) Principal Features of ENDOR Spectra. Figure 5 shows four selected proton ENDOR spectra recorded at the observing field values marked by arrows in Figure 2. They all exhibit the following features: (i) a set of more or less resolved lines localized at the proton nuclear frequency $\nu_0 = g_N\beta_N B_0$, representing the dipolar interactions of the unpaired electron spin on the metal with the protons of the solvent cage (the so-called matrix line[28]); (ii) several pairs of lines (one, two or three, depending on the field setting) at $\nu_0 \pm A/2$ due to the hf interaction of the unpaired electron spin with protons of C_7H_7 rings. The ENDOR spectra strongly depend on the field setting

(26) Simanek, E.; Sroubek, Z. *Electron Paramagnetic Resonance*; Plenum Press: New York, 1972; p 535.

(27) McConnell, H. M.; Chesnut, D. B. *J. Chem. Phys.* **1958**, *28*, 107.

(28) Hyde, J. S.; Rist, G. H.; Eriksson, L. E. G. *J. Phys. Chem.* **1968**, *72*, 4269.

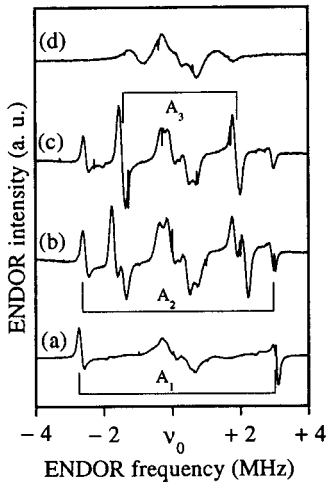

Figure 5. Four selected ENDOR spectra at 4 K recorded at the field setting values marked by arrows in Figure 2. These spectra correspond to particular molecular orientations where some of the ENDOR frequencies give approximately the hf parameters A_1, A_2, and A_3.

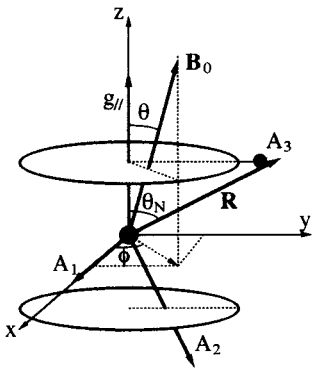

Figure 6. The principal axis system of the g and hf tensors.

value, which is the indication of a good selection of molecular orientations. This arises because the intrinsic EPR line width of the spin packets representing each individual molecular orientation is very small (typically 2.5 mT for a spectral width of 250 mT).

The general features of the ENDOR spectra can be qualitatively understood by considering the relation between the g and A tensor axes. Figure 6 is a schematic representation of a sandwich complex, with a proton at a distance R from the metal atom and the U−H axis at polar angles θ_N and ϕ_N in the g frame. The z axis of the axial g tensor being parallel to the molecular axis, if the EPR spectrum is partially saturated at a field setting $B_0 = h\nu/g\beta$ located between the parallel and perpendicular turning points and characterized by the g value $g(\theta) = (g_{||}^2 \cos^2\theta + g_{\perp}^2 \sin^2\theta)^{1/2}$, this implies that the selected set of molecular orientations makes an angle θ with the magnetic field $\mathbf{B}_0$ (see Figure 2). However the principal axes of the g and A tensors are not collinear (Figure 6), and the A_3 axis of the hf interaction with one hydrogen points approximately toward this atom, and thus makes an angle close to θ_N with the $g_{||}$ tensor axis (the molecular axis). The consequence is that if a single molecular orientation θ is selected, the other polar angle ϕ can assume all the possible values between 0 and 360° because of the axial symmetry of the g tensor. For this reason the ENDOR spectrum is a powder average of all the possible values of ϕ, and presents a characteristic powder line shape with one, two or three turning points for each m_s state.[17,18,29] Owing to the possible symmetries D_{7d} or C_{2h} of **1**,with C_2 axes perpendicular to z, one of the hf principal axis (chosen as the A_1 axis) is perpendicular to z.

(29) Gourier, D.; Samuel, E. *J. Am. Chem. Soc.* **1987**, *109*, 4571.

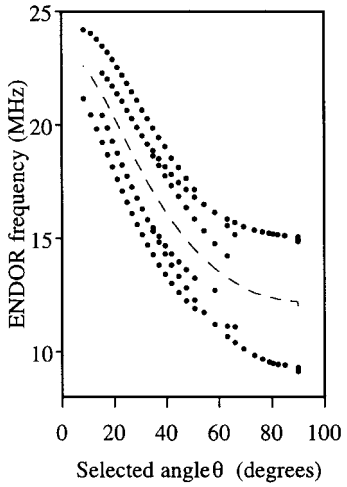

Figure 7. Frequencies of the ENDOR turning points versus the selected molecular orientations. The selected angle θ is given by expression 15. The discontinuous line represents the variation of the proton nuclear frequency ν_0.

Let us now consider the ENDOR spectrum of Figure 5d, obtained with the field setting d of Figure 2. In this case the selected molecules have their axis at about 8° from the magnetic field $\mathbf{B}_0$, and the protons are almost magnetically equivalent. For $\mathbf{B}_0||z$ (i.e. $\theta = 0$) we expect only two symmetrical (single crystal like) ENDOR lines at frequencies $\nu_{\pm} \approx \nu_0 \pm A(\theta_N)/2$. However the ENDOR signal is very weak in that case. This is the reason we choose a field setting below the parallel turning point, which gives a stronger ENDOR intensity. For the field setting a of Figure 2 giving the ENDOR response of Figure 5a, all the selected molecular axes make an angle $\theta = \pi/2$ with $\mathbf{B}_0$. We expect ENDOR lines with two sets of turning points corresponding to A_1 and $A_2' \approx A_2 \cos^2\theta_N + A_3 \sin^2\theta_N$. Figure 5a clearly shows the turning points at $\nu_{\pm} \approx \nu_0 \pm A_1/2$, the other turning points at $\nu_{\pm} \approx \nu_0 \pm A_2'/2$ being hindered by the matrix lines.[30] The two other ENDOR spectra of Figure 5 correspond to selected molecular axes making an angle $\theta \approx \pi/2 - \theta_N$ (Figure 5b) and $\theta \approx \theta_N$ (Figure 5c). In these cases the spectra exhibit turning points at $\nu_{\pm} \approx \nu_0 \pm A_2/2$ and $\nu_{\pm} \approx \nu_0 \pm A_3/2$ respectively.

(2) Measurement of the Proton Hyperfine Parameters. To test this qualitative interpretation and thus to obtain accurate values of the proton hf parameters, we performed a "crystallographic ENDOR" study by taking advantage of the good angular selection of molecular orientations resulting from the small EPR line width. Figure 7 shows the variation of ENDOR frequencies versus the selected angle θ, related to the field B_0 by

$$\theta = \cos^{-1}\left[\frac{(h\nu/\beta B_0)^2 - g_{\perp}^2}{g_{||}^2 - g_{\perp}^2}\right]^{1/2} \qquad (15)$$

The important angular variation of ENDOR frequencies arises both from the angular dependence of the proton hf tensor $\bar{\bar{\mathbf{A}}}$ and the B_0 dependence of the nuclear frequency $\nu_0 = g_N\beta_N B_0/h$. Since the latter is known (discontinuous line in Figure 7), it is possible to extract the hf tensor $\bar{\bar{\mathbf{A}}} = (A_1, A_2, A_3)$ expressed in its principal axis system. However the selection of molecular

(30) The weak symmetrical lines close to the turning points cannot be interpreted as allowed $\Delta m_s = 0$, $\Delta m_I = \pm 1$ ENDOR transitions.

angle θ is made in the reference frame of the g tensor $\bar{\bar{\mathbf{g}}} = (g_1,g_2,g_3)$ with $g_3 = g_{||}$ and $g_1 = g_2 = g_\perp$, and the hf tensor is not diagonal in this frame. Hurst et al. derived a general expression for the first-order ENDOR frequencies in a general situation of non coaxial g and A tensors:[18]

$$\nu(m_s) = \left[\sum_{i=1}^{3}\left[\frac{m_s}{g(\theta)}\left(\sum_{j=1}^{3} g_j h_j A_{ji}\right) - h_i \nu_0\right]^2\right]^{1/2} \tag{16}$$

with $m_s = \pm^1/_2$ and with $h_1 = \cos\phi \sin\theta$, $h_2 = \sin\phi \sin\theta$, and $h_3 = \cos\theta$ being the director cosines of the field $\mathbf{B}_0$. The elements A_{ji} of the hf tensor are expressed in the g frame and are related to the elements A_{kl} in the A-frame by

$$[A_{ji}] = \mathbf{P}^{-1}[A_{kl}]\mathbf{P} \tag{17a}$$

where

$$\mathbf{P} = \begin{bmatrix} 1 & 0 & 0 \\ 0 & \cos\theta_N & -\sin\theta_N \\ 0 & \sin\theta_N & \cos\theta_N \end{bmatrix} \tag{17b}$$

is the rotation matrix around g_1 (|| A_1) by an angle θ_N. Theoretical expressions of the angular variations of ENDOR frequencies can be derived from expressions 16 and 17. Since the powder ENDOR line shape exhibits turning points corresponding to the polar angles $\phi = 0$ and $\phi = \pi/2$, we shall consider these two situations separately. For the case $\phi = 0$, corresponding to a rotation of the field in the (g_3,g_1) plane, we obtain the following expression relating the ENDOR frequencies $\nu(m_s)$ to the hf parameters A_1, A_2, and A_3:

$$g^2(\theta)\nu^2(m_s) = x_1 \sin^2\theta + x_2 \cos^2\theta \tag{18a}$$

with

$$x_1 = (m_s A_1 g_\perp - g(\theta)\nu_0)^2$$

and

$$x_2 = (m_s(A_3 - A_2)g_{||} \sin\theta_N \cos\theta_N)^2 \tag{18b}$$

$$+ (m_s(A_2 \sin^2\theta_N + A_3 \cos^2\theta_N)g_{||} - g(\theta)\nu_0)^2$$

Alternatively an angular variation in the (g_3,g_2) plane, characterized by $\phi = \pi/2$, gives the expressions:

$$g^2(\theta)\nu^2(m_s) = (x_3 \sin\theta + x_4 \cos\theta)^2 + (x_5 \sin\theta + x_6 \cos\theta)^2 \tag{19a}$$

with

$$x_3 = m_s g_\perp (A_2 \cos^2\theta_N + A_3 \sin^2\theta_N) - g(\theta)\nu_0$$

$$x_4 = m_s g_{||}(A_3 - A_2)\sin\theta_N \cos\theta_N$$

$$x_5 = m_s g_\perp (A_3 - A_2)\sin\theta_N \cos\theta_N$$

$$x_6 = m_s g_{||}(A_2 \sin^2\theta_N + \cos^2\theta_N) - g(\theta)\nu_0 \tag{19b}$$

Figure 8 represents the experimental and calculated angular dependences of $g^2(\theta)\nu^2(m_s)$ for the two polar angles $\phi = 0$ (open circles) and $\phi = \pi/2$ (full circles). The theoretical curves have been calculated from eqs 18 and 19, with the angle $\theta_N = 43.9°$ and the hf parameters $A_1 = \pm 5.8(5)$ MHz, $A_2 = \pm 5.5(9)$ MHz and $A_3 = \mp 3.3(3)$ MHz. It must be noted that A_3 and (A_1,A_2) are of opposite signs. The relatively good agreement between experimental and calculated curves confirms the qualitative interpretation proposed for the ENDOR spectra of Figure 5. The observed discrepancies could be due to second-order effects, which are not accounted for in expression 16.

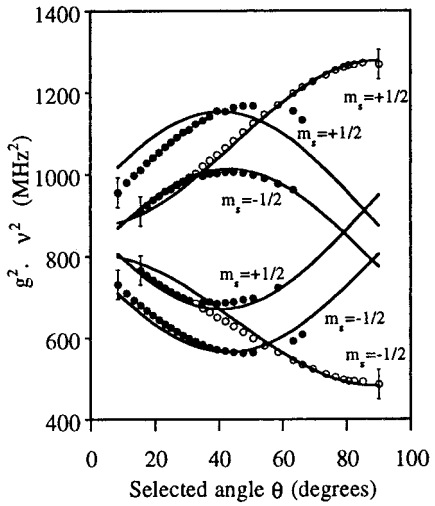

Figure 8. Variation of $g^2(\theta)\nu(\theta)^2$ versus the selected angle. The full and empty circles correspond to the turning points $\phi = \pi/2$ and $\phi = 0$, respectively. Error bars are only indicated for some experimental points for the sake of clarity. The full lines are calculated with expressions 18 and 19.

The proton hf interaction can be separated into the isotropic (scalar) part A_{iso} and the anisotropic (traceless tensor) part A_i^{aniso}:

$$A_{iso} = \frac{1}{3}\sum_{i=1}^{3} A_i$$

$$A_i^{aniso} = A_i - A_{iso} \tag{20}$$

with $A_{iso} = \pm 2.7(0)$ MHz, $A_1^{aniso} = \pm 3.1(5)$ MHz, $A_2^{aniso} = \pm 2.8(9)$ MHz, and $A_3^{aniso} = \mp 6.0(3)$ MHz. It is worth noticing that the anisotropic terms are comparable with those calculated from a pure dipole−dipole hf interaction, given by the following expression:

$$A^{dd}(\theta) = \frac{g\beta g_N \beta_N}{hR^3}[3\cos^2(\theta_N - \theta) - 1] \tag{21}$$

Taking the value $R = 3.25$ Å for the uranium−hydrogen distance,[13] expression 21 gives $A_3^{dd} = +4.60$ MHz and $A_1^{dd} = A_2^{dd} = -2.30$ MHz for $\theta = \theta_N$ and $\theta = \theta_N - \pi/2$ respectively (by considering $g > 0$). Although these values are different from the experimental values of A_i^{aniso}, they are close enough to imply that they are of the same sign, which gives only one possibility for the sign of the hf parameters (Table 2).

(3) Ligand Contribution to the SOMO. The important information given by ENDOR is that the isotropic proton hf interaction is negative. This corresponds to a negative spin density $\rho_H = -1.9 \times 10^{-3}$ at each hydrogen atom, which indicates a covalent character of the SOMO of **1**. For example, the value $A_{iso} = -2.70$ MHz found for **1** is close to the value $A_{iso} = -2.4$ MHz found for the $Co(Cp)_2$ complex ($Cp = \eta^5$-C_5H_5), with a SOMO presenting a pronounced metal−Cp

covalent interaction.[31] Alternatively a SOMO made of the nonbonding d_σ (d_{z^2}) orbital in transition metal sandwich complexes exhibits a large and positive value of A_{iso} due to the direct delocalization of the unpaired electron spin in 1s hydrogen orbital. For example Ti(Cp)(cht)$^-$ anion (cht = η^7-C_7H_7) is characterized by $A_{iso} = +14.2$ MHz for the hf interaction with C_7H_7 protons.[32] The fact that **1** exhibits a negative isotropic proton hf interaction close to that of $(Cp)_2Co$ is sufficient to conclude that its SOMO shows a significant covalent interaction with the C_7H_7 rings.

This conclusion must be refined by a more quantitative analysis of the hyperfine parameters. The negative sign of the isotropic hf interaction A_{iso} in a sandwich complex results from the spin polarization of the inner σ(CH) orbitals due to a nonzero spin density at the $2p_\pi$ AO of the ring carbon atoms (Figure 4) and also to a direct f_σ-1s(H) interaction. Thus the isotropic interaction with the *i*th proton is written as the sum of two terms:

$$A_{iso}^{(i)} = Q_1 \rho_\pi^{(i)} + a_H^2 A_{iso}^H \qquad (22)$$

The first term represents the contribution from the spin polarization given by the McConnell relation,[27] where $\rho_\pi^{(i)}$ is the spin density in the $2p_\pi$ AO of the *i*th carbon. The parameter Q_1 is the hf interaction for an isolated CH fragment, with $Q_1 = -76.28$ MHz for η^7-C_7H_7 ring.[33] The second term of 22 represents the direct $f_\sigma-1s(H)$ interaction, where $A_{iso}^H = +1420$ MHz is the hf interaction for an isolated hydrogen atom and a_H^2 is the spin density at the hydrogen nucleus, a_H being the coefficient of the 1s hydrogen AO in the SOMO. This contribution is the largest one for transition metal sandwich complexes with a SOMO made of the nonbonding d_{z^2} ($d\sigma$) orbital,[34] and the SOMO of **1** contains 39% of $5f_\sigma$ uranium orbital (see expression 10). However the lobes of the f_σ orbital are more slender than those of the d_σ orbital, so that the overlap with hydrogen 1s should be weaker. For this reason, the direct metal−hydrogen interaction is probably very weak in **1**, because even a very small a_H coefficient should give an important positive contribution to A_{iso}. For example a spin density as small as $a_H^2 = 10^{-4}$ should contribute to +0.14 MHz to the isotropic hf interaction. Since we ignore the value of a_H, expression 22 with $a_H = 0$ gives only a lower limit for ρ_π. Neglecting the slight inequivalence of carbon atoms due to the staggered ring conformation, an average spin density $\rho_\pi \geq +0.036$ in each carbon $2p_\pi$ AO is obtained. This value is similar to that found for cobaltocene ($\rho_\pi = +0.078$), which possesses a $3d_\pi$-based SOMO with a pronounced contribution of π-MOs of Cp rings.[31]

Returning to Figure 4, the positive sign of ρ_π and its magnitude indicate that there is a direct covalent transfer between π-based ligand MOs and the singly occupied f-based orbital. It appears that both ligand to half-filled metal transfer (mechanism a) and metal to empty ligand transfer (back-bonding mechanism c) can contribute to the covalent character of the SOMO. In axial symmetry (D_{7h}, D_{7d}, and D_7) and neglecting the spin−orbit interaction,[14] the filled a_2'' and e_1' ligand MO can interact with f_σ and f_π uranium orbitals by mechanism a. Also the empty e_3' ligand MO can interact with the f_ϕ orbital by the back-bonding mechanism c.[7] Since f_σ and f_π orbitals contribute to 90% to the SOMO, compared to 9% for the f_ϕ orbital, it appears that a ligand to half-filled metal AO transfer appears as the dominant mechanism of covalence for the SOMO, which should thus exhibit an antibonding character.

Concluding Remarks

The $S = {}^1/_2$ character of $[U(\eta^7\text{-}C_7H_7)_2]^-$ anion **1** gives the opportunity to explore the nature of the SOMO, its covalent character, and to get information on the f-level ordering by EPR and ENDOR. The association of these techniques with photoelectron and optical spectroscopies as well as theoretical calculations, should now make it possible to analyze the complete energy level diagram of this family of compounds.

Spin−orbit effects strongly influence the part of the energy level diagram containing the f-based MOs. The analysis of the EPR parameters indicates that both the strong participation of the $5f_\delta$ orbitals to the bonding and the spin−orbit coupling could be responsible for the actual f composition of the SOMO. The latter was found to be composed essentially of 51% of $5f_\pi$ and 39% of $5f_\sigma$ uranium orbitals, a composition close to that of a purely $J = {}^5/_2$, $M_j = \pm{}^1/_2$ doublet. The small admixture of $5f_\phi$ orbitals might be due to a low symmetry effect resulting from the conjunction of the staggered ring conformation of **1**, solid-state packing forces, and the very small splitting between the SOMO and f_ϕ orbitals. In this context the extremely small admixture of $5f_\delta$ orbitals is due to its important separation from the SOMO resulting from its participation to the bonding.

From our analysis it can be proposed that the dominant $J = {}^5/_2$, $M_j = \pm{}^1/_2$ ground state and the very poor f_δ admixture constitute a fingerprint of a strong participation of the latter orbitals to the bonding. Curiously enough, the composition of the SOMO of **1** is similar to that recently found for a series of organouranium(V) compounds,[35] which all exhibit a predominant $J = {}^5/_2$, $M_j = \pm{}^1/_2$ ground state, regardless of their geometry (pseudotetrahedra or trigonal bipyramids) and the nature of their ligands. This result might indicate that these compounds also exhibit a significant participation of the f_δ orbitals to the bonding.

Finally it also appears that ENDOR spectrocopy opens the possibility of exploring the ligand character of the f_σ-, f_π-, and f_ϕ-based MOs usually considered as nonbonding in **1** and in actinocenes.[2−9,14] In particular this techniques gives an estimate of the spin density mapping on the ligand atoms of the complex. Since these parameters are observable quantities that can be estimated by MO calculations, it might be useful that future works dealing with theoretical calculations on paramagnetic uranium compounds systematically indicate the spin densities at metal and ligand atoms.

Acknowledgment. We are grateful to Mrs. Simmons for technical assistance.

JA9740172

(31) Rudin, M.; Fauth, J. M.; Schweiger, A.; Ernst, R. R.; Zoller, L.; Ammeter, J. H. *Mol. Phys.* **1983**, *49*, 1257.
(32) Gourier, D.; Samuel, E. *Inorg. Chem.* **1988**, *27*, 3018.
(33) Carrington, A.; Smith, I. C. P. *Mol. Phys.* **1963**, *7*, 99.
(34) Rieger, P. H. *Coord. Chem. Rev.* **1994**, *135/136*, 203.
(35) Gourier, D.; Caurant, D.; Berthet, J. C.; Boisson, C.; Ephritikhine, M. *Inorg. Chem.* **1997**, *36*, 5931.